Journal of Integrative Neuroscience

J. Integr. Neurosci. **2026**; 25(3): 48953
https://doi.org/10.31083/JIN48953

Original Research

Miro1 Mediates the Neuroprotective Effects of Electroacupuncture Against Cerebral Ischemia-Reperfusion Injury in Mice

Huidan Lian[1,†], Yan Sun[2,†], Minyuan Zhang[1], Xiangying Gao[1], Junlu Wang[1], Qinxue Dai[1,*]

[1]Department of Anesthesia, The First Affiliated Hospital of Wenzhou Medical University, 325000 Wenzhou, Zhejiang, China
[2]The Second Clinical Medical College, Wenzhou Medical University, 325000 Wenzhou, Zhejiang, China
*Correspondence: daiqinxue@wzhospital.cn (Qinxue Dai)
[†]These authors contributed equally.
Academic Editor: Hahn Young Kim
Submitted: 9 December 2025 Revised: 28 February 2026 Accepted: 3 March 2026 Published: 25 March 2026

Abstract

Background: Cerebral ischemia-reperfusion injury (CIRI) is a severe neurological condition where restoring neuronal mitochondrial function critically impacts prognosis. While electroacupuncture (EA) has demonstrated neuroprotective effects by improving mitochondrial function, the precise underlying mechanisms remain unclear. Emerging evidence suggests that astrocyte-to-neuron mitochondrial transfer, facilitated by mitochondrial Rho-GTPase 1 (Miro1), serves as a vital neuroprotective pathway. Therefore, this study investigates whether astrocytic Miro1 participates in the neuroprotective effects of EA against CIRI in mice by regulating the expression of the mitochondrial marker translocase of the outer mitochondrial membrane 40 (TOM40) and adenosine triphosphate (ATP) levels in damaged neurons. **Methods**: 126 C57BL/6 mice were randomly allocated into seven experimental groups (n = 18 per group): Sham-operated (Sham), middle cerebral artery occlusion (MCAO) model, EA, sham electroacupuncture (SEA), EA combined with astrocyte-specific Miro1 knockdown (GFAP: glial fibrillary acidic protein, EA+AAV-GFAP-shMiro1), astrocyte-specific Miro1 over-expression (AAV-GFAP-hiMiro1), and adenoviral empty vector control (AAV-GFAP-control). The CIRI model was induced using MCAO. Prior to model induction, the EA group received pretreatment with EA at the Baihui (GV20) acupoint. The SEA group underwent identical procedures to the EA group except for electrical stimulation. For the EA+AAV-GFAP-shMiro1, AAV-GFAP-hiMiro1, and AAV-GFAP-control groups, mice received intracerebroventricular injections of AAV-GFAP-shMiro1, AAV-GFAP-hiMiro1, or AAV-GFAP-control, respectively, 48 hours prior to EA treatment, with other procedures matching the EA group. At 24 hours post-reperfusion, neurological deficit scores, cerebral infarct volume, and neuronal survival in the peri-infarct penumbra were assessed. Astrocytes and neurons from the peri-infarct penumbra were isolated to measure ATP levels and expression of the mitochondrial-specific protein TOM40 in neurons, as well as ATP levels, TOM40, and Miro1 protein expression in astrocytes. **Results**: Relative to the Sham group, the MCAO group displayed a significant increase in cerebral infarct volume and neurological deficit scores, accompanied by a marked reduction in neuronal viability, TOM40 expression, and ATP levels ($p < 0.01$). In contrast to the MCAO and SEA groups, the EA and AAV-GFAP-hiMiro1 groups demonstrated improved neurological scores, reduced infarct volume, enhanced neuronal viability, elevated neuronal ATP levels and TOM40 expression, as well as decreased astrocytic ATP and TOM40 levels, but significantly increased Miro1 expression in astrocytes ($p < 0.01$). When compared to the EA group, the EA+AAV-GFAP-shMiro1 group exhibited a reversal of all the aforementioned improvements ($p < 0.01$), while the AAV-GFAP-hiMiro1 group showed no significant changes ($p > 0.05$). **Conclusions**: EA exerts neuroprotective effects in MCAO mice by upregulating Miro1 protein expression in astrocytes and upregulating the mitochondrial marker TOM40 alongside ATP levels in neurons. Silencing Miro1 abolished the neuroprotective effects of EA and reduced neuronal TOM40 expression, while Miro1 overexpression increased this mitochondrial marker and mimicked EA-mediated neuroprotection. These findings identify Miro1 as a key effector of EA-induced neuroprotection, although the upstream signaling pathways linking EA to Miro1 upregulation require further investigation.

Keywords: electroacupuncture; mitochondrial transfer; GTP phosphohydrolases; reperfusion injury; brain ischemia; neuroprotection

1. Introduction

Cerebral infarction represents a common neurological disorder affecting the central nervous system. It is distinguished by its elevated occurrence frequency, significant fatality risk, and substantial impairment potential, thereby constituting a serious global health concern [1]. Mitochondria are critical organelles that regulate cellular homeostasis and function through energy metabolism, calcium signaling, cellular metabolism, and apoptosis [2]. During cerebral ischemia-reperfusion injury (CIRI), the restoration of mitochondrial function in neurons profoundly impacts stroke prognosis [3,4]. During electroacupuncture (EA) intervention, a sparse-dense wave at a frequency of 2/15 Hz was applied for stimulation at the Baihui (GV20) acupoint. The choice of this parameter is based on the classical "frequency-specific effect" theory, which posits that

different electrical stimulation frequencies can activate distinct endogenous neurochemical pathways [5]. Specifically, the 2/15 Hz pattern is designed to integrate the potential benefits of low-frequency (2 Hz) and medium-to-high-frequency (15 Hz) stimulation, thereby exerting synergistic neuroprotective effects through multi-target mechanisms [6]. Studies have shown that EA improves mitochondrial function in neurons of rats with middle cerebral artery occlusion (MCAO), contributing to its neuroprotective effects [7,8]. However, the underlying mechanisms remain unclear.

Hayakawa *et al*. [9] utilized transgenic mice with fluorescently labeled astrocytes to establish an MCAO model, observing fluorescently tagged mitochondria within damaged neurons in the peri-infarct penumbra, suggesting that astrocytes transfer their mitochondria to injured neurons, thus implicating mitochondrial transfer as a neuroprotective mechanism. Furthermore, Tseng *et al*. [10] demonstrated that the upregulation of mitochondrial Rho-GTPase 1 (Miro1) expression in mesenchymal stem cells enhances the intercellular transfer of mitochondria to oxidant-damaged neurons, thereby improving neuronal metabolism and survival. Conversely, decreasing Miro1 expression was found to impair this mitochondrial transfer capacity and diminish the neuroprotective benefits. Building on these insights, it is hypothesized that EA at Baihui may promote astrocyte-to-neuron mitochondrial transfer via astrocytic Miro1, thereby mediating neuroprotection.

To investigate this hypothesis, this study employed an MCAO mouse model combined with adeno-associated viruses carrying glial fibrillary acidic protein (GFAP) specific promoters to either over-express or silence Miro1 in astrocytes. The effects of EA on mitochondrial quantity and function were evaluated in neurons and astrocytes. The aim was to elucidate novel mechanisms underlying EA-induced neuroprotection.

2. Materials and Methods

2.1 Animals

Male C57BL/6 mice (20–25 g) were procured from Beijing Vital River Laboratory Animal Technology (China). These animals were maintained, with food and water *ad libitum*, in controlled laboratory environments. Prior to surgical procedures, a 24-hour fasting period, withdrawal of both food and water, was enforced. The entire experimental protocol and animal care procedures followed the ethical standards established by the First Affiliated Hospital of Wenzhou Medical University.

2.2 Reagents and Instruments

1% 2,3,5-triphenyltetrazolium chloride (TTC) staining reagent (Cat# C0651, Beyotime Biotechnology Co., Ltd., Shanghai, China); Isoflurane (Cat# R510-22-2, RWD Life Science Co., Ltd., Shenzhen, Guangdong, China); Brain matrix (Cat# 68707, RWD Life Science Co., Ltd.); AAV-GFAP-hiMiro1 (Genewiz Biotech Co., Ltd., Guangzhou, Guangdong, China); AAV-GFAP-control (Genewiz Biotech Co., Ltd.); AAV-GFAP-shMiro1 (Genewiz Biotech Co., Ltd.); Acupuncture needles (Size: 0.18 $\times$ 13 mm, Suzhou Medical Appliance Factory Co., Ltd., Suzhou, Jiangsu, China); Han's EA apparatus (Model HANS-200A, Jisheng Medical Technology Co., Ltd., Nanjing, Jiangsu, China); Stereotaxic instrument (Cat# 68801, RWD Life Science Co., Ltd.); 4% paraformaldehyde (Cat# BL539A, Biosharp Life Sciences, Hefei, Anhui, China); Mouse neuron (Cat# 130-115-389, Miltenyi Biotec, Bergisch Gladbach, North Rhine-Westphalia, Germany) and astrocyte (Cat# 130-097-678, Miltenyi Biotec) magnetic bead sorting kits, MS MACS columns (Cat# 130-042-201, Miltenyi Biotec), and autoMACS Pro separator (Cat# 130-092-545, Miltenyi Biotec, Bergisch Gladbach, North Rhine-Westphalia, Germany). The primary antibodies targeting MAP2 (Cat# ab221693, Abcam, Cambridge, Cambridgeshire, UK), the outer mitochondrial membrane 40 (TOM40; Cat# ab185543, Abcam) , Miro1 (Cat# ab188029, Abcam) and Alexa Fluor 594-conjugated secondary antibody (Cat# ab150068, Abcam). The anti-rabbit IgG, HRP-conjugated secondary antibodies (Cat# 7074, Cell Signaling Technology, Danvers, MA, USA). ATP Bioluminescence Assay Kit CLS II (Cat# 11699695001, Roche, Basel, Switzerland). BCA protein assay (Cat# 23227, Thermo Fisher Scientific, Waltham, MA, USA).

2.3 MCAO Model

Anesthesia was induced via inhalation of 5% isoflurane and maintained with 2% isoflurane. Following hair removal and sterilization of the cervical region, a midline incision was performed in the neck area using microsurgical techniques. The internal carotid artery (ICA), external carotid artery, and right common carotid artery were isolated. A blunt-tipped monofilament suture was then introduced into the right ICA and carefully advanced until reaching the middle cerebral artery origin to induce vascular occlusion. Following a two-hour ischemic period, the suture was removed to restore cerebral blood flow, after which the surgical wound was closed. Neurological function was evaluated using standardized scoring criteria after recovery from anesthesia, with animals scoring below one point being excluded from subsequent analysis. Core body temperature was maintained at 37.0 $\pm$ 0.2 °C during the entire experimental procedure via continuous rectal monitoring [11].

2.4 Experimental Grouping

126 C57BL/6 mice were randomly divided into seven groups (n = 18 per group) using a randomized block design, including: Sham operation group (Sham), model group (MCAO), EA, sham EA group (SEA), EA + astrocytic Miro1 knockdown group (EA+AAV-GFAP-shMiro1), astrocytic Miro1 overexpression group (AAV-GFAP-hiMiro1) and adenoviral empty vector control group (AAV-GFAP-control).

2.5 Intervention Methods

2.5.1 Electroacupuncture (EA) Intervention

The Baihui acupoint (GV20) was located at the intersection of the line connecting the two ear tips and the sagittal midline in mice [12]. After localization, an acupuncture needle was inserted approximately 1 mm into the Baihui acupoint. Another needle was inserted into the left forelimb (non-acupoint site) as the return electrode to complete the circuit. The Han's EA device was employed to administer electrical stimulation under controlled conditions, with specific settings including a dual-frequency mode (2/15 Hz), current strength set at 1 mA, and a treatment period lasting 30 minutes.

2.5.2 Intracerebroventricular (ICV) Injection

For the respective experimental groups, ICV injections of AAV-GFAP-shMiro1, AAV-GFAP-hiMiro1, or AAV-GFAP-control (1 µL per mouse) were performed 48 h prior to EA treatment. The infusion procedure was conducted at a constant flow rate of 0.2 µL per minute, with the entire administration process completed within five minutes. For the intracerebroventricular (ICV) delivery, the stereotactic positioning parameters were established at 0.4 mm caudal to bregma, with a 1 mm lateral deviation from the midline and a penetration depth of 2 mm [13].

2.6 Isolation of Astrocytes and Neurons From the Peri-Infarct Penumbra in Mice Using Magnetic-Activated Cell Sorting (MACS)

2.6.1 Tissue Preparation

Following a 24-hour period after CIRI, mice were deeply anesthetized via inhalation of 3% isoflurane in an oxygen/air mixture and subsequently euthanized by decapitation. The penumbral region surrounding the infarct area was isolated and mechanically dissociated in chilled phosphate-buffered saline (PBS) utilizing pipette techniques. Tissue digestion was performed using a 0.25% trypsin solution, after which the enzymatic reaction was halted by introducing a stop solution. Subsequent centrifugation at 300 ×g for 10 minutes under 4 °C conditions allowed for supernatant removal, yielding a purified single-cell suspension preparation.

2.6.2 Neuron Isolation

A suspension of 1×10^7 cells was prepared in 80 µL of MACS buffer supplemented with 20 µL of biotin-labeled antibodies directed against non-neuronal cell populations. The mixture was maintained at 4 °C for a five-minute incubation period. Subsequently, 1 mL of MACS buffer was added to the sample, which was then centrifuged at 300 ×g for 10 minutes. The supernatant was then carefully removed. The resulting cell pellet was reconstituted in 80 µL of MACS buffer combined with 20 µL of anti-biotin microbeads, followed by incubation at 4 °C for 10 minutes. The cell suspension was then loaded onto a pre-wetted MACS column in the autoMACS separator. After sequential steps of pre-wetting, loading, and washing, the flow-through fraction (neurons) that did not adhere to the column was collected.

2.6.3 Astrocyte Isolation

To prepare the cell suspension, 1×10^7 cells were mixed with 80 µL of MACS buffer supplemented with 20 µL of ACSA-1 microbeads (astrocyte-specific surface antibody-1), and the mixture was incubated at 4 °C for five minutes. Subsequently, 1 mL of MACS buffer was added to the suspension, which was then centrifuged at 300 ×g for 10 minutes. The supernatant was discarded, and the cell suspension was loaded onto a pre-wetted MACS column in the autoMACS separator. After loading and washing, the column retained positive cells (astrocytes). To verify the morphological characteristics of the isolated primary cells, a fraction of the sorted cell suspension was cultured and observed under a phase-contrast microscope. The isolated neurons exhibited typical distinct, rounded somas with long, extending neurites. In contrast, the sorted astrocytes displayed characteristic stellate or polygonal morphologies with multiple extended branching processes, consistent with typical primary astrocyte morphology.

2.7 Assessment Parameters and Methods

2.7.1 Neurological Deficit Scoring

Neurological function was evaluated at 24 h post-reperfusion using a standardized scoring system, the Longa 5-point scale [11]. 0: No neurological deficits, 1: Failure to fully extend contralateral forelimb; 2: Circling toward the contralateral side; 3: Falling to the contralateral side; 4: Loss of spontaneous movement with impaired consciousness. All assessments were performed by an experimenter blinded to the group allocations.

2.7.2 Cerebral Infarct Volume Measurement

24 hours after reperfusion, mice were deeply anesthetized via inhalation of 3% isoflurane in an oxygen mixture prior to decapitation for brain tissue collection. The harvested cerebral tissues were rapidly frozen at –20 °C for 20 minutes, followed by coronal sectioning into four sequential 2 mm thick slices utilizing a specialized brain matrix apparatus. These tissue sections were subsequently immersed in a 1% solution of TTC staining reagent and maintained at 37 °C for precisely 20 minutes during the incubation process. Viable tissue stained red, while infarcted areas remained pale. Images were scanned and analyzed using a LUZEX-F image analysis system (Nireco Corporation, Tokyo, Japan). Infarct volume was calculated using the Swanson method to correct for brain edema. Briefly, the areas of the contralateral hemisphere and the non-infarcted ipsilateral hemisphere were measured on each slice. Infarct volume percentage was calculated as: (contralateral hemisphere volume – ipsilateral non-infarcted volume) / contralateral hemisphere volume × 100%.

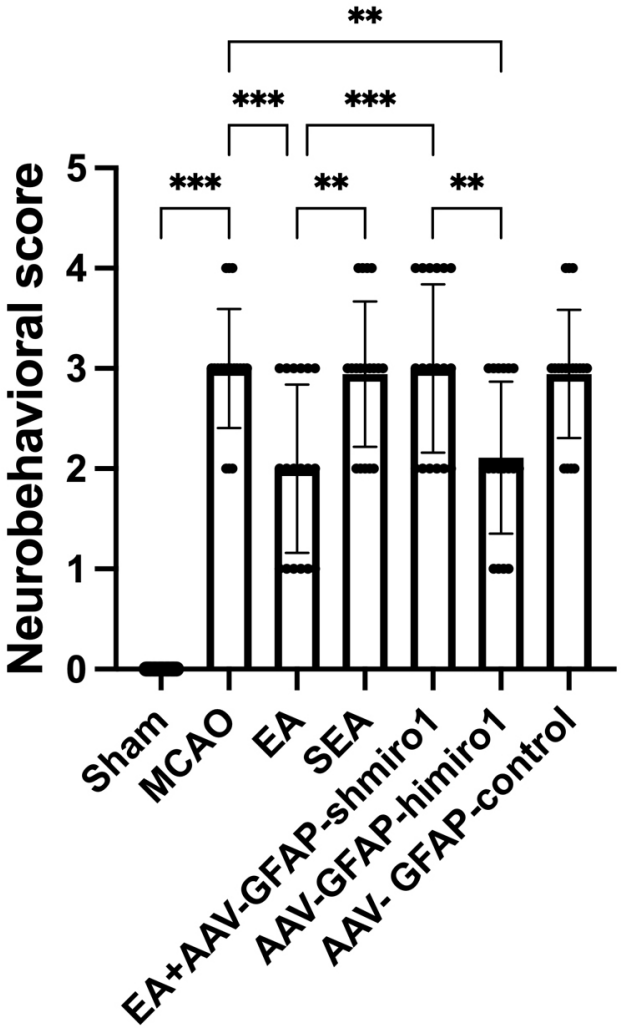

Fig. 1. Comparison of neurological deficit scores among experimental groups (n = 18 per group). Data are presented as mean ± SD. $^{**}p < 0.01$, $^{***}p < 0.001$ vs. respective control groups as indicated in the text; one-way ANOVA followed by Fisher's least significant difference (LSD) *post hoc* test for parametric data, Kruskal–Wallis test with Nemenyi's *post hoc* test for non-parametric scores. Sham, Sham surgery; MCAO, Model group; EA, Electroacupuncture; SEA, Sham electroacupuncture; EA + AAV-GFAP-shMiro1, EA + astrocytic Miro1 knockdown; AAV-GFAP-hiMiro1, Astrocytic Miro1 overexpression; AAV-GFAP-control, Adenoviral empty vector control.

2.7.3 Immunofluorescence Assessment of Surviving Neurons in the Peri-Infarct Penumbra

24 hours after CIRI, mice underwent anesthesia and were subjected to transcardial perfusion using 4% paraformaldehyde solution. Harvested brain tissues were subsequently embedded in paraffin blocks for histological preparation. After deparaffinization, coronal sections 3.5 µm thick were treated with 3% hydrogen peroxide solution for 10 minutes to inhibit endogenous peroxidase activity. For antigen retrieval, tissue sections were heated in 10 mmol/L citrate buffer (pH 6.0) for 20 minutes, followed by gradual cooling to ambient temperature. Prior to primary antibody incubation, sections were blocked with PBS containing 5% bovine serum albumin for one hour at room temperature. The primary antibody employed was rabbit anti-MAP2 (1:500 dilution, ab221693, Abcam), which was applied overnight at 4 °C. Following three PBS washes, sections were exposed to Alexa Fluor 594-conjugated secondary antibody (1:500 dilution, ab150068, Abcam) for one hour at room temperature. Nuclear counterstaining was performed using 4′,6-diamidino-2-phenylindole (DAPI, 1 µg/mL concentration) for five minutes. After final PBS rinses, prepared slides were coverslipped and examined under an Olympus BX51 fluorescence microscope (Olympus Corporation, Tokyo, Japan) with standardized imaging parameters (including gain, threshold, and black level settings), maintained throughout all experimental procedures. Quantification of viable neurons was based on the identification of cells exhibiting a $MAP2^+$ (red fluorescence) signal surrounded by $DAPI^+$ (blue) nuclear staining. For statistical analysis, five randomly selected microscopic fields (×400 magnification) per section were evaluated to determine the mean number of surviving neurons.

2.7.4 ATP Content Measurement in Neurons and Astrocytes

The isolated neurons and astrocytes underwent lysis, after which intracellular ATP concentrations were measured utilizing a commercially available ATP detection system (ATP Bioluminescence Assay Kit CLS II, Roche) based on the luciferin-luciferase reaction. In this procedure, cellular lysates were combined with the enzyme substrate solution, followed by immediate luminescence detection performed with a microplate luminometer. To standardize the measurements, ATP quantities were adjusted according to the total protein levels quantified through the BCA protein assay, with results presented in units of nmol per milligram of protein.

2.7.5 Western Blot Analysis of TOM40 and Miro1 Protein Expression

To prepare protein samples, neuronal or astrocytic cells were solubilized using 1% Triton X-100 lysis buffer, followed by protein concentration determination through BCA protein assay. For electrophoretic analysis, identical protein quantities (5 µg) were loaded onto SDS-polyacrylamide gel wells. After electrophoretic separation, proteins were transferred onto nitrocellulose membranes using wet transfer methodology. Membrane blocking was performed with 5% skim milk dissolved in tris-buffered saline (TBST) containing 0.1% Tween-20 for 60 minutes at ambient temperature. Subsequently, membranes were probed with primary antibodies targeting TOM40 (dilution 1:5000) and Miro1 (dilution 1:1000) overnight at 4 °C. Following TBST washes, membranes were exposed to HRP-

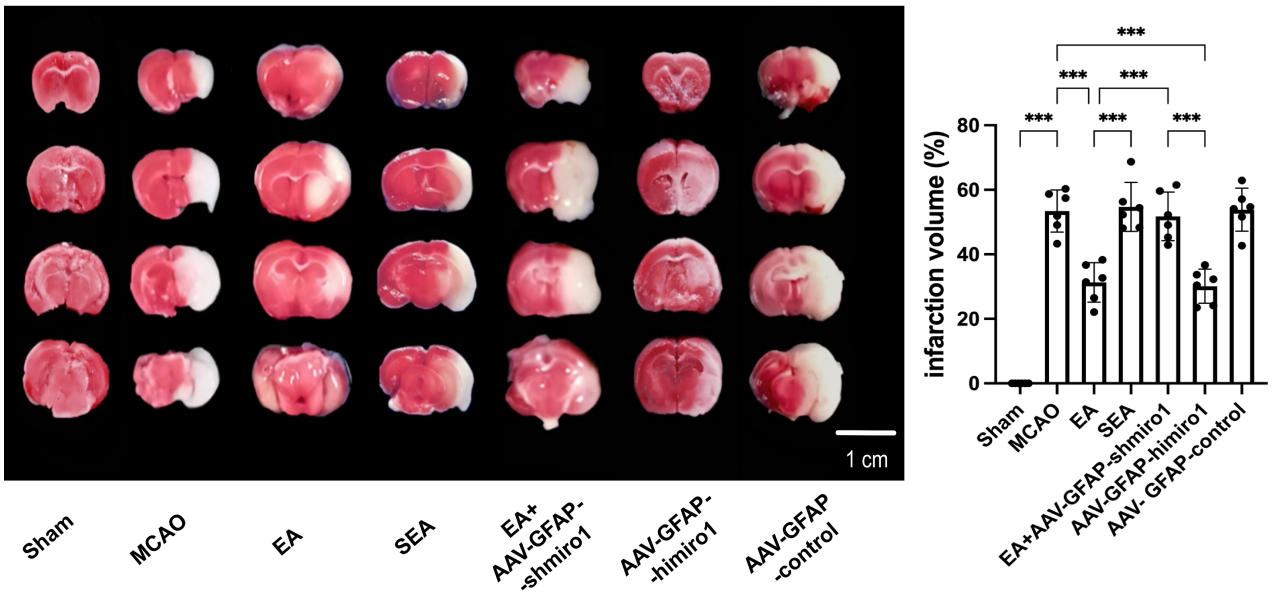

Fig. 2. Comparison of cerebral infarct volume measured by 2,3,5-triphenyltetrazolium chloride (TTC) staining across experimental groups (n = 6, randomly selected from 18 per group). Data are presented as mean ± SD. ***$p < 0.001$ vs. respective control groups as indicated in the text. Statistical analysis was performed by one-way ANOVA followed by the LSD *post hoc* test. Scale = 1 cm.

conjugated secondary antibodies (1:5000 dilution) for one hour at room temperature. Protein detection was achieved through enhanced chemiluminescence reaction, with signal capture on Kodak X-Omat AR radiographic film (Eastman Kodak Company, Rochester, NY, USA). Quantitative analysis of band intensities was conducted using ImageJ software (Version 1.54g, National Institutes of Health, Bethesda, MD, USA). Representative Western blot images are shown in the main figures, and the corresponding original, uncropped blots are provided in the **Supplementary Material**.

2.8 Statistical Analysis

All statistical analyses and graph construction were performed using GraphPad Prism software (Version 10.1.0, GraphPad Software, San Diego, CA, USA). Continuous variables with normal distribution were presented as mean ± standard deviation (SD). For comparisons among multiple groups, one-way ANOVA was initially employed, supplemented by Fisher's least significant difference (LSD) tests for detailed pairwise analysis. Regarding neurological deficit scoring data, which exhibited non-parametric distribution characteristics, the Kruskal-Wallis test was implemented, with subsequent Nemenyi tests facilitating specific group comparisons. Statistical significance was defined as a p-value less than 0.05.

3. Results

3.1 Comparison of Neurological Deficit Scores Across Experimental Groups

As shown in Fig. 1, the neurological deficit scores were significantly elevated in the MCAO group when compared with the Sham group ($p < 0.001$). Conversely, the EA treatment group exhibited significantly decreased scores relative to both the MCAO and SEA groups ($p < 0.001$). The AAV-GFAP-hiMiro1 group also presented with significantly lower scores than the MCAO group ($p < 0.001$). Nevertheless, the EA+AAV-GFAP-shMiro1 combination group manifested significantly higher scores than either the EA or AAV-GFAP-hiMiro1 groups alone ($p < 0.001$). Statistical analysis revealed no significant difference between either the EA and AAV-GFAP-hiMiro1 groups or between the MCAO and AAV-GFAP-control groups.

3.2 Comparison of Cerebral Infarct Volume Among Experimental Groups

As shown in Fig. 2, the infarct size was significantly greater in the MCAO group when compared with the Sham-operated controls ($p < 0.001$). Conversely, EA treatment resulted in a significant decrease in infarct area relative to both the MCAO and SEA groups ($p < 0.001$). The AAV-GFAP-hiMiro1 intervention similarly led to significantly diminished infarct volumes versus the MCAO group ($p < 0.001$). Notably, the combined EA+AAV-GFAP-shMiro1 treatment group exhibited significantly larger infarct areas than either the EA or AAV-GFAP-hiMiro1 groups alone ($p < 0.001$). Statistical analysis revealed no significant vari-

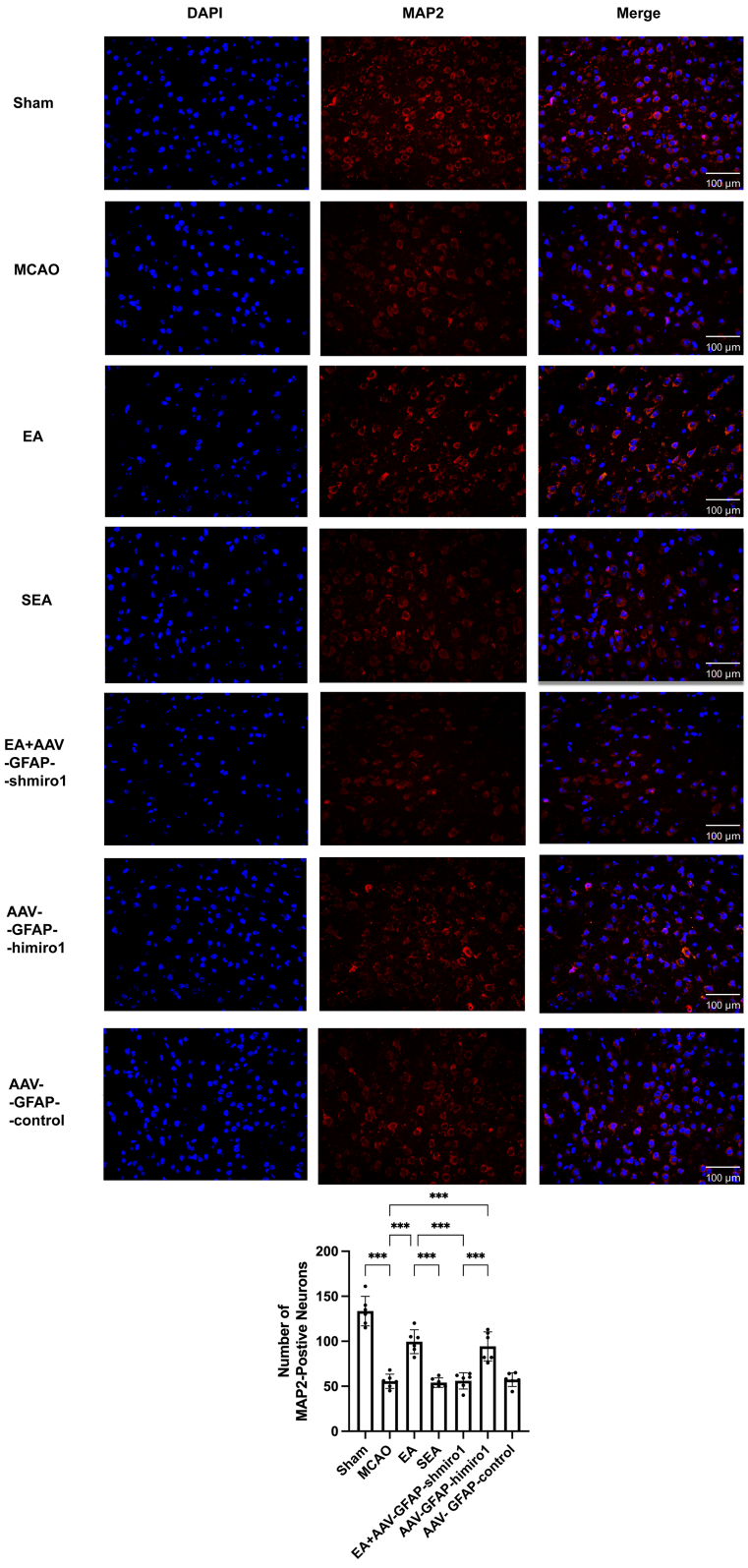

Fig. 3. Comparison of neuronal viability in the peri-infarct penumbra across experimental groups (immunofluorescence staining, ×400 magnification; *n* = 6, randomly selected from 18 per group). Data are presented as mean ± SD. ***$p < 0.001$ vs. respective control groups as indicated in the text. Statistical analysis was performed by one-way ANOVA followed by the LSD *post hoc* test. Scale = 100 μm.

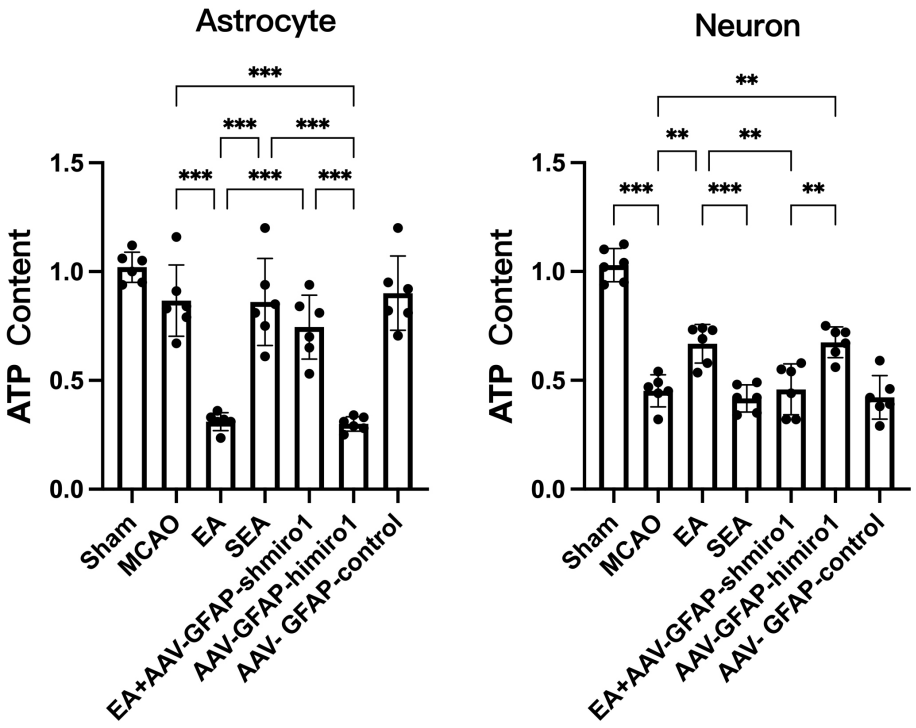

Fig. 4. Comparison of ATP levels in neurons and astrocytes across experimental groups (bioluminescence assay; $n = 6$, randomly selected from 18 per group). Data are presented as mean ± SD. $^{**}p < 0.01$, $^{***}p < 0.001$ vs. respective control groups as indicated in the manuscript. Statistical analysis was performed by one-way ANOVA followed by the LSD *post hoc* test.

ations in infarct volume between either the EA and AAV-GFAP-hiMiro1 groups or the MCAO and AAV-GFAP-control groups.

3.3 Comparison of Neuronal Viability in the Peri-Infarct Penumbra Across Experimental Groups

As shown in Fig. 3, neuronal survival rates in the peri-infarct penumbra were significantly lower in the MCAO group when compared with the Sham operated controls ($p < 0.001$). Conversely, EA treatment resulted in significantly increased neuronal survival compared to both the MCAO and SEA groups ($p < 0.001$). The AAV-GFAP-hiMiro1 intervention group also exhibited significant enhancement in neuronal viability relative to the MCAO group ($p < 0.001$). However, the combination treatment group (EA+AAV-GFAP-shMiro1) showed significantly reduced neuronal viability when compared with either EA or AAV-GFAP-hiMiro1 treatment alone ($p < 0.001$). Statistical analysis revealed no significant differences in neuronal viability between either the EA and AAV-GFAP-hiMiro1 groups or the MCAO and AAV-GFAP-control groups.

3.4 Comparison of ATP Levels in Neurons and Astrocytes Across Experimental Groups

As shown in Fig. 4, neuronal ATP concentrations in the peri-infarct penumbra were substantially lower in the MCAO group than in the Sham group ($p < 0.001$), whereas astrocytic ATP levels remained statistically unchanged. The EA treatment group presented with significantly higher neuronal ATP content and lower astrocytic ATP content when compared to both MCAO and SEA groups ($p < 0.001$). Parallel results were observed in the AAV-GFAP-hiMiro1 group, which exhibited enhanced neuronal ATP production and diminished astrocytic ATP levels relative to the MCAO group ($p < 0.001$). Conversely, the EA+AAV-GFAP-shMiro1 combination group demonstrated reduced neuronal ATP concentrations and elevated astrocytic ATP levels in comparison to both EA and AAV-GFAP-hiMiro1 groups ($p < 0.001$). Statistical analysis revealed no significant variations in ATP content between EA and AAV-GFAP-hiMiro1 groups or between MCAO and AAV-GFAP-control groups, in either neuronal or astrocytic populations.

3.5 Comparison of TOM40 and Miro1 Protein Expression in Astrocytes Across Experimental Groups

As illustrated in Fig. 5, the MCAO group showed no significant changes in TOM40 or Miro1 protein expression in astrocytes of the peri-infarct penumbra compared to the Sham group. In contrast, the EA group exhibited significantly increased Miro1 expression and decreased TOM40 levels in astrocytes compared to both the MCAO and SEA groups ($p < 0.001$). Similarly, the AAV-GFAP-hiMiro1 group demonstrated significantly elevated Miro1 expression and reduced TOM40 levels relative to the MCAO group ($p < 0.001$). However, the EA+AAV-GFAP-shMiro1

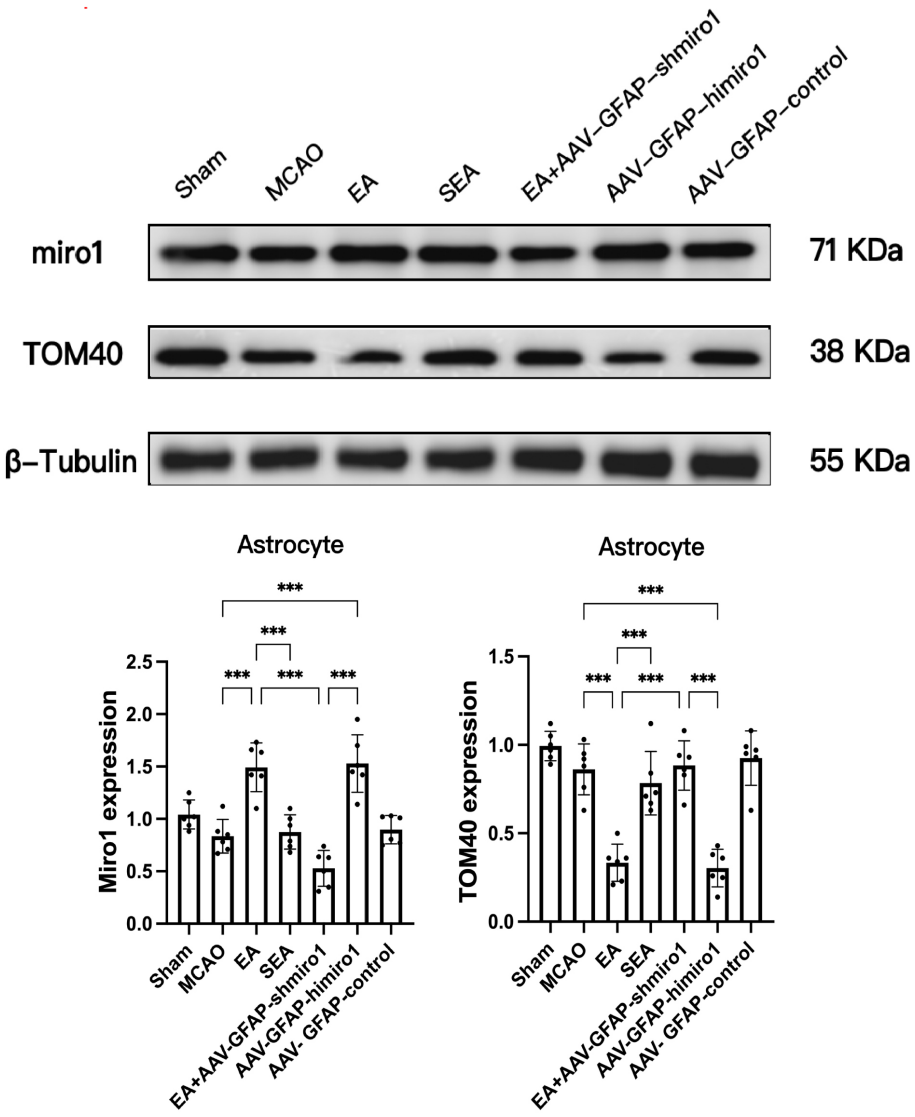

Fig. 5. Comparison of TOM40 and Miro1 protein expression in astrocytes across experimental groups (Western blot analysis; *n* = 6, randomly selected from 18 per group). Data are presented as mean ± SD. ***$p < 0.001$ vs. respective control groups as indicated in the text. Statistical analysis was performed by one-way ANOVA followed by the LSD *post hoc* test.

group displayed significantly reduced Miro1 expression and increased TOM40 levels compared to both the EA and AAV-GFAP-hiMiro1 groups ($p < 0.001$). No significant differences in TOM40 or Miro1 expression were found between either the EA and AAV-GFAP-hiMiro1 groups or between the MCAO and AAV-GFAP-control groups ($p > 0.001$).

3.6 Comparison of TOM40 Expression in Neurons Across Experimental Groups

As illustrated in Fig. 6, the MCAO group exhibited significantly reduced TOM40 expression in neurons of the peri-infarct penumbra compared to the Sham group ($p < 0.001$). In contrast, the EA group demonstrated significantly increased TOM40 expression relative to both the MCAO and SEA groups ($p < 0.001$). Similarly, the AAV-GFAP-hiMiro1 group showed significantly elevated TOM40 expression compared to the MCAO group ($p < 0.001$). However, the EA+AAV-GFAP-shMiro1 group displayed significantly decreased TOM40 expression compared to both the EA and AAV-GFAP-hiMiro1 groups ($p < 0.001$). No significant differences in neuronal TOM40 expression were observed between the EA and AAV-GFAP-hiMiro1 groups or between the MCAO and AAV-GFAP-control groups.

4. Discussion

As the predominant glial cell population in the central nervous system, astrocytes perform essential functions in modulating synaptic activity, upholding blood-brain barrier integrity, facilitating synaptic plasticity, and ensuring neuronal stability [14]. During cerebral ischemic events, these

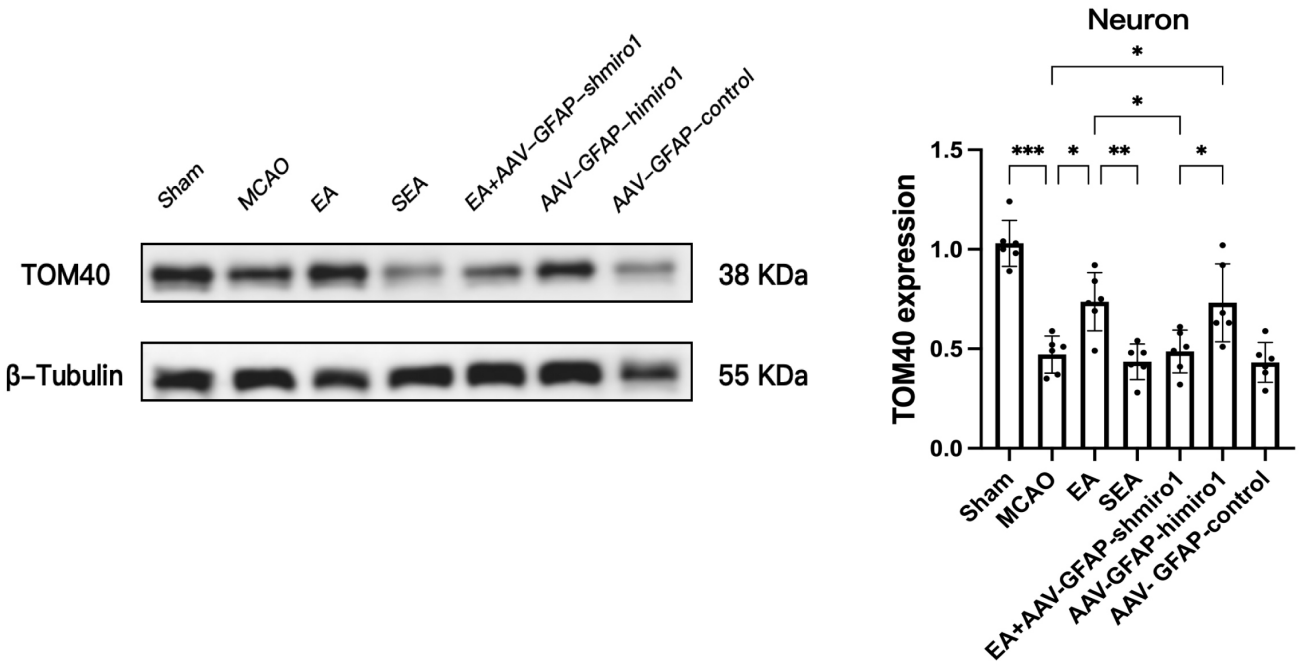

Fig. 6. Comparison of TOM40 expression in neurons across experimental groups (Western blot analysis; $n = 6$, randomly selected from 18 per group). Data are presented as mean ± SD. *$p < 0.05$, **$p < 0.01$, ***$p < 0.001$ vs. respective control groups as indicated in the manuscript. Statistical analysis was performed by one-way ANOVA followed by the LSD *post hoc* test.

cells exhibit reactive changes marked by cellular hypertrophy and elevated production of GFAP, phenomena strongly correlated with ischemic neuronal injury [15]. Following ischemic stroke, astrocytes exert multifaceted neuroprotective effects [16]. For instance, astrocytic scar formation around ischemic lesions isolates damaged areas from healthy tissue, shielding surviving neurons from harmful substances released by the infarct core [17]. Thus, astrocytes are pivotal for post-stroke recovery.

The mechanisms governing mitochondrial transfer remain incompletely understood. Key players include the motor protein KIF5 and the adaptor protein Miro1/2, which mediate mitochondrial transport [18]. Miro1, a calcium-sensitive protein anchored to the mitochondrial outer membrane, binds KIF5 to form a transport complex [18,19]. This complex facilitates mitochondrial transfer between cells via tunneling nanotubes (TNTs) [19,20], which are extensively distributed between astrocytes and neurons [21] with their connectivity intensifying under ischemic conditions and enhancing intercellular communication and tissue repair [22]. In neurons, Miro1 governs mitochondrial trafficking; its deficiency disrupts mitochondrial distribution and motility, contributing to neurological disorders [23]. Notably, studies suggest that peri-infarct astrocytes transfer functional mitochondria to ischemic neurons, promoting neuronal survival [9]. It is hypothesized here that during CIRI, astrocytes export mitochondria to damaged neurons via Miro1-mediated TNTs, thereby exerting neuroprotection.

This study investigated whether EA enhances astrocyte-to-neuron mitochondrial transfer via Miro1 to mitigate CIRI. Compared to the Sham group, MCAO mice exhibited enlarged infarct volumes, worsened neurological deficits, and reduced neuronal ATP/TOM40 levels, while astrocytic ATP/TOM40 remained unchanged. This indicates severe mitochondrial dysfunction in neurons but preserved mitochondrial integrity in astrocytes, likely due to astrocytic glycogen storage and superior hypoxia tolerance [16]. EA significantly increased astrocytic Miro1 expression while reducing astrocytic ATP/TOM40 and elevating neuronal ATP/TOM40, correlating with improved neurological outcomes and reduced infarct volume. These findings suggest EA promotes mitochondrial transfer from astrocytes to neurons.

Mechanistically, astrocyte-specific Miro1 knockdown (AAV-GFAP-shMiro1) abolished EA-induced increases in neuronal ATP/TOM40 and reversed EA's neuroprotective effects. Conversely, astrocytic Miro1 overexpression (AAV-GFAP-hiMiro1) mimicked EA's benefits, confirming Miro1's essential role. Critically, viral controls (AAV-GFAP-control) did not alter outcomes, excluding nonspecific viral effects. These results strongly support that EA upregulates astrocytic Miro1 to enhance mitochondrial export to neurons via TNTs, restoring neuronal ATP levels and the expression of mitochondrial biogenesis markers.

We fully acknowledge that this study has several limitations. First, although our findings strongly suggest that EA promotes astrocyte-to-neuron mitochondrial transfer via Miro1, direct evidence using TNT inhibitors is lacking,

and the proposed mechanism remains hypothetical. Second, the specific transduction pathways linking the physical stimulus (EA) to the molecular signal (Miro1 upregulation) have not been elucidated. This represents a core gap in the current mechanistic framework. Based on existing literature and preliminary clues, we propose the following testable hypotheses: (1) EA may induce Ca^{2+} transients in astrocytes, activating calcineurin-nuclear factor of activated T-cells (NFAT) or calcium/calmodulin-dependent protein kinase (CaMK)-cAMP response element-binding protein (CREB) pathways to promote Miro1 transcription [24,25]; (2) EA stimulation at Baihui (GV20) may trigger neuronal glutamate release, activating astrocytic metabotropic glutamate receptors 3/5 (mGluR3/5) receptors and downstream signaling cascades [26,27]; (3) EA-induced adaptive oxidative stress may regulate Miro1 expression via the nuclear factor erythroid 2-related factor 2-antioxidant response element (Nrf2-ARE) pathway [28]. All of these hypotheses require rigorous experimental validation in future studies. We have planned subsequent investigations using *in vitro* co-culture systems combined with pathway-specific inhibitors, chromatin immunoprecipitation-quantitative polymerase chain reaction (ChIP-qPCR), and other techniques to systematically dissect the molecular mechanisms by which EA regulates Miro1.

Furthermore, regarding the assessment of mitochondria, we used TOM40 protein expression alongside ATP levels to evaluate neuronal mitochondrial status. It should be noted that changes in TOM40 levels may primarily reflect mitochondrial biogenesis or protein assembly processes, rather than serving as a direct equivalent of total mitochondrial mass or content. To definitively confirm an increase in absolute mitochondrial content, future studies employing direct methods such as mitochondrial DNA quantification or electron microscopic morphometry are warranted.

5. Conclusions

This study demonstrates that EA may protect against CIRI by upregulating astrocytic Miro1 to boost mitochondrial transfer to neurons, thereby contributing to the restoration of neuronal mitochondrial function and biogenesis markers. These findings unveil a novel astrocyte-dependent mechanism of EA-mediated neuroprotection, offering potential therapeutic targets for ischemic stroke.

Availability of Data and Materials

The datasets used and analysed during the current study available from the corresponding author on reasonable request.

Author Contributions

HL: Writing – original draft, Validation, Conceptualization. YS: Validation, Formal analysis, Writing – original draft. MZ: Writing – original draft, Validation, Conceptualization. XG: Investigation, Data curation, Writing – review & editing. JW: Conceptualization, Formal analysis, Writing – review & editing, Resources. QD: Writing – review & editing, Supervision, Conceptualization, Project administration. All authors read and approved the final manuscript. All authors have participated sufficiently in the work and agreed to be accountable for all aspects of the work.

Ethics Approval and Consent to Participate

All animal care and experiments were conducted according to the Institutional Animal Care and Use Committee of Wenzhou Medical University, and all experiments were designed to minimize animal suffering. The study protocol was approved by the Animal Experiment Committee of Wenzhou Medical University (WYYY-AEC-2021-295).

Acknowledgment

We would like to express our gratitude to all those who helped us during the writing of this manuscript. Thanks to all the peer reviewers for their opinions and suggestions.

Funding

This study was supported by the Natural Science Foundation of China (Nos.81704180).

Conflict of Interest

The authors declare no conflict of interest.

Supplementary Material

Supplementary material associated with this article can be found, in the online version, at https://doi.org/10.31083/JIN48953.

References

[1] Go AS, Mozaffarian D, Roger VL, Benjamin EJ, Berry JD, Blaha MJ, *et al*. Heart disease and stroke statistics–2014 update: a report from the American Heart Association. Circulation. 2014; 129: e28–e292. https://doi.org/10.1161/01.cir.0000441139.02102.80.

[2] Harrington JS, Ryter SW, Plataki M, Price DR, Choi AMK. Mitochondria in health, disease, and aging. Physiological Reviews. 2023; 103: 2349–2422. https://doi.org/10.1152/physrev.00058.2021.

[3] Yang JL, Mukda S, Chen SD. Diverse roles of mitochondria in ischemic stroke. Redox Biology. 2018; 16: 263–275. https://doi.org/10.1016/j.redox.2018.03.002.

[4] Zhou L, Wang Y, Qiao J, Wang QM, Luo X. Acupuncture for Improving Cognitive Impairment After Stroke: A Meta-Analysis of Randomized Controlled Trials. Frontiers in Psychology. 2020; 11: 549265. https://doi.org/10.3389/fpsyg.2020.549265.

[5] Han JS. Acupuncture: neuropeptide release produced by electrical stimulation of different frequencies. Trends in

Neurosciences. 2003; 26: 17–22. https://doi.org/10.1016/s0166-2236(02)00006-1.

[6] Wang Q, Xiong L, Chen S, Liu Y, Zhu X. Rapid tolerance to focal cerebral ischemia in rats is induced by preconditioning with electroacupuncture: window of protection and the role of adenosine. Neuroscience Letters. 2005; 381: 158–162. https://doi.org/10.1016/j.neulet.2005.02.019.

[7] Guo Y, Fu T, Cheng Y, Li Y, Zhang R, Ma Q, *et al*. Mechanisms of electroacupuncture-induced neuroprotection in acute stroke rats: the role of astrocyte-mediated mitochondrial transfer. Cell Communication and Signaling: CCS. 2025; 23: 316. https://doi.org/10.1186/s12964-025-02287-9.

[8] Kim JH, Choi KH, Jang YJ, Bae SS, Shin BC, Choi BT, *et al*. Electroacupuncture acutely improves cerebral blood flow and attenuates moderate ischemic injury via an endothelial mechanism in mice. PloS One. 2013; 8: e56736. https://doi.org/10.1371/journal.pone.0056736.

[9] Hayakawa K, Esposito E, Wang X, Terasaki Y, Liu Y, Xing C, *et al*. Transfer of mitochondria from astrocytes to neurons after stroke. Nature. 2016; 535: 551–555. https://doi.org/10.1038/nature18928.

[10] Tseng N, Lambie SC, Huynh CQ, Sanford B, Patel M, Herson PS, *et al*. Mitochondrial transfer from mesenchymal stem cells improves neuronal metabolism after oxidant injury in vitro: The role of Miro1. Journal of Cerebral Blood Flow and Metabolism. 2021; 41: 761–770. https://doi.org/10.1177/0271678x20928147.

[11] Longa EZ, Weinstein PR, Carlson S, Cummins R. Reversible middle cerebral artery occlusion without craniectomy in rats. Stroke. 1989; 20: 84–91. https://doi.org/10.1161/01.str.20.1.84.

[12] Guo Y. Appendix: Common acupuncture points in experimental animals. In Guo Y (ed.) Experimental Acupunctology (pp. 414–417). 1st edn. China Press of Traditional Chinese Medicine: Beijing. 2008. (In Chinese).

[13] Fukushima A, Fujii M, Ono H. Intracerebroventricular Treatment with Resiniferatoxin and Pain Tests in Mice. Journal of Visualized Experiments: JoVE. 2020; 163. https://doi.org/10.3791/57570.

[14] Potokar M, Morita M, Wiche G, Jorgačevski J. The Diversity of Intermediate Filaments in Astrocytes. Cells. 2020; 9: 1604. https://doi.org/10.3390/cells9071604.

[15] Su H, Fan S, Zhang L, Qi H. TMAO Aggregates Neurological Damage Following Ischemic Stroke by Promoting Reactive Astrocytosis and Glial Scar Formation *via* the Smurf2/ALK5 Axis. Frontiers in Cellular Neuroscience. 2021; 15: 569424. https://doi.org/10.3389/fncel.2021.569424.

[16] Jia J, Jin H, Nan D, Yu W, Huang Y. New insights into targeting mitochondria in ischemic injury. Apoptosis: an International Journal on Programmed Cell Death. 2021; 26: 163–183. https://doi.org/10.1007/s10495-021-01661-5.

[17] Zamanian JL, Xu L, Foo LC, Nouri N, Zhou L, Giffard RG, *et al*. Genomic analysis of reactive astrogliosis. The Journal of Neuroscience. 2012; 32: 6391–6410. https://doi.org/10.1523/JNEUROSCI.6221-11.2012.

[18] Birsa N, Norkett R, Higgs N, Lopez-Domenech G, Kittler JT. Mitochondrial trafficking in neurons and the role of the Miro family of GTPase proteins. Biochemical Society Transactions. 2013; 41: 1525–1531. https://doi.org/10.1042/BST20130234.

[19] Gao L, Zhang Z, Lu J, Pei G. Mitochondria Are Dynamically Transferring Between Human Neural Cells and Alexander Disease-Associated GFAP Mutations Impair the Astrocytic Transfer. Frontiers in Cellular Neuroscience. 2019; 13: 316. https://doi.org/10.3389/fncel.2019.00316.

[20] Fransson S, Ruusala A, Aspenström P. The atypical Rho GTPases Miro-1 and Miro-2 have essential roles in mitochondrial trafficking. Biochemical and Biophysical Research Communications. 2006; 344: 500–510. https://doi.org/10.1016/j.bbrc.2006.03.163.

[21] Wang X, Bukoreshtliev NV, Gerdes HH. Developing neurons form transient nanotubes facilitating electrical coupling and calcium signaling with distant astrocytes. PloS One. 2012; 7: e47429. https://doi.org/10.1371/journal.pone.0047429.

[22] Wang Y, Cui J, Sun X, Zhang Y. Tunneling-nanotube development in astrocytes depends on p53 activation. Cell Death and Differentiation. 2011; 18: 732–742. https://doi.org/10.1038/cdd.2010.147.

[23] Nguyen TT, Oh SS, Weaver D, Lewandowska A, Maxfield D, Schuler MH, *et al*. Loss of Miro1-directed mitochondrial movement results in a novel murine model for neuron disease. Proceedings of the National Academy of Sciences of the United States of America. 2014; 111: E3631–E3640. https://doi.org/10.1073/pnas.1402449111.

[24] Kim JH, Choi KH, Jang YJ, Kim HN, Bae SS, Choi BT, *et al*. Electroacupuncture preconditioning reduces cerebral ischemic injury via BDNF and SDF-1α in mice. BMC Complementary and Alternative Medicine. 2013; 13: 22. https://doi.org/10.1186/1472-6882-13-22.

[25] Ding S. Ca(2+) signaling in astrocytes and its role in ischemic stroke. Advances in Neurobiology. 2014; 11: 189–211. https://doi.org/10.1007/978-3-319-08894-5_10.

[26] Guo F, Song W, Jiang T, Liu L, Wang F, Zhong H, *et al*. Electroacupuncture pretreatment inhibits NADPH oxidase-mediated oxidative stress in diabetic mice with cerebral ischemia. Brain Research. 2014; 1573: 84–91. https://doi.org/10.1016/j.brainres.2014.05.020.

[27] Panatier A, Robitaille R. Astrocytic mGluR5 and the tripartite synapse. Neuroscience. 2016; 323: 29–34. https://doi.org/10.1016/j.neuroscience.2015.03.063.

[28] Dirnagl U, Becker K, Meisel A. Preconditioning and tolerance against cerebral ischaemia: from experimental strategies to clinical use. The Lancet. Neurology. 2009; 8: 398–412. https://doi.org/10.1016/S1474-4422(09)70054-7.